Int. J. Electrochem. Sci., 15 **(2020)** 1412 – 1425, doi: 10.20964/2020.02.25

International Journal of
ELECTROCHEMICAL
SCIENCE
www.electrochemsci.org

Expired Drug Theophylline as Potential Corrosion Inhibitor for 7075 Aluminium Alloy in 1M NaOH Solution

Peng Su[1], *Lintao Li*[1], *Weiliang Li*[1], *Chuanyan Huang*[1], *Xiaohong Wang*[2,*], *Hao Liu*[2], *Ambrish Singh*[2,*]

[1] Research Institute of Engineering Technology, SINOPEC Northwest Oilfield Company, Urumqi-830011, China.
[2] School of Material Science and Engineering (Southwest Petroleum University), Chengdu, Sichuan 610500, China.
[*]E-mail: vishisingh4uall@gmail.com; xhwang3368@swpu.edu.cn

Received: 26 September 2019 / *Accepted:* 22 November 2019 / *Published:* 31 December 2019

The expired drug Theophylline (DT) was used as impending corrosion inhibitor for 7075 aluminium in saline environment. The investigations were done using gravimetric tests, electrochemical tests, surface characterizations, and quantum calculations. Gravimetric tests were done with respect to time, temperature and inhibitor concentration. The studies showed the good efficiency in presence of DT. Electrochemical tests included impedance and polarization studies. Impedance results showed the surge in charge transfer resistance values with rise in DT concentration. Localized electrochemical behavior was determined using scanning electrochemical microscopy (SECM). SECM showed the inductive surface in presence of DT and conductive in it absence. Surface characterization tests consist of contact angle, and scanning electrochemical microscopy (SEM). Quantum simulations were done using Gaussian 9.0 software using density functional theory (DFT) to get computational parameters that can support the experimental findings. All the results showed that the Theophylline drug can inhibit the 7075 aluminium alloy in saline media effectively.

Keywords: Aluminium alloy; Corrosion; Inhibition; SEM; SECM; DFT

1. INTRODUCTION

One of the cheap and reliable metals used today is aluminium and its alloys due to its better strength with density proportion. It serves a large number of applications including transportation, aviation, two-wheelers, hiking gear, inline skating-frames and hang glider frames [1-5]. The high demand of aluminium and its alloys in the industries is however concerned with its corrosion resistance in aggressive medium. Aluminium is known for its pragmatic applications due to the natural protection through the oxide layer that further deteriorates in the corrosive medium.

As one of the known fact states the poor performance of aluminum in alkaline mediums. Lower corrosion resistance is seen in sodium and potassium hydroxide solutions while higher resistance can be seen in ammonium hydroxide mediums for numerous aluminum samples. The higher resistance can be attributed to the presence of 4 wt.% Mg in the aluminium metal. Aluminium is exposed to alkaline mediums in batteries and etching process where corrosion can lead to several problems. In batteries corrosion can lead to the self-discharge due to corrosion of aluminium metal [6-11].

The mechanism of aluminium immersed in alkaline medium was studied broadly using electrochemical methods [12]. The mechanism includes the formation of a hydroxide layer which further disseminates due to anodic reaction. Is was established formerly that this layer is molded due to the movement of the hydroxide ions on the metal surface.

$$Al + 3OH^- = Al(OH)_3 + 3e^- \quad (1)$$

The formed aluminum hydroxide layer is then broken by the outbreak of the hydroxide ions to form solvable aluminate ions.

$$Al(OH)_3 + OH^- = Al(OH)_4^- \quad (2)$$

The Eq. (1) and Eq. (2) together provides the partial anodic dissolution reaction of pure aluminum in alkaline solutions, as can be represented in Eq. (3):

$$Al + 4OH^- = Al(OH)_4^- + 3e^- \quad (3)$$

Two possible cathodic reactions can occur including reduction of water and/or reduction of oxygen as can be signified by Eqs. (4) and (5):

$$3/4O_2 + 3/2H_2O + 3e^- = 3OH^- \quad (4)$$

$$3/2H_2O + 3e^- = 3/2H_2 + 3OH^- \quad (5)$$

The corrosion process can be shortened by combining Eqs. (3) and (4):

$$Al + OH^- + 3/4O_2 + 3/2H_2O = Al(OH)_4^- \quad (6)$$

and/or by merging Eqs. (3) and (5):

$$Al + 3H_2O + OH^- = 3/2H_2 + Al(OH)_4^- \quad (7)$$

The evolution of bubbles formed due to corrosion of aluminium in alkaline solution vindicates that the dissolution of aluminum goes generally by the reduction of water [13].

Previous works have indicated the good potential of organic compounds as inhibitors to mitigate corrosion [14-16]. The organic compounds contain π bonds, benzene rings, conjugated double bonds, and heteroatoms (N, S, O, P) that makes them very efficient. A wide class of drugs have similar structures to these carbon-based complexes including pyridines, furans, imidazoles, thiophenes, isoxazoles etc [17-20]. This distinguished feature is the motivation worldwide to study the potential of drugs as corrosion inhibitors. Being eco-friendly, and non-toxic, drugs ideally suit the environmental regulations over the toxic inhibitors. Therefore, a number of research work is done using new and expired medications as corrosion inhibitors [21-25]. The outcome of using the expired drugs were surprising as they prove to be ideal and cost effective corrosion inhibitors than being a pharmaceutical compound that needs to be disposed of [26-28].

In present study we have used expired drug Theophylline (DT) commonly known as 1,3-dimethylxanthine, is a drug of methylxanthine category beneficial for breathing illnesses like chronic obstructive pulmonary disease (COPD) besides asthma as shown in Fig. 1. It is only available as a

generic drug in the form of oral tablet, capsule or oral solution. The structure and pharmacological behavior of Theophylline (DT) is similar to that of theobromine and caffeine. This is due to the fact that they all belong to the Xanthine family. It originates freely in nature and can be located in tea (Camellia sinensis) and cocoa (Theobroma cacao). Theophylline (DT) is lone product of caffeine metabolism in the liver. The drug is non-toxic and can help in opening up of the lung airways. It does it by relaxing the muscles and making it easier to breathe.

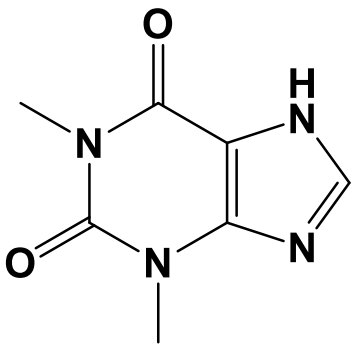

Figure 1. Structure of 1,3-dimethylxanthine (Theophylline drug).

2. EXPERIMENTAL

2.1. Preparation of inhibitor

The expired Theophylline (DT) drug tablets were purchased from the pharmacy. It was weighed and powdered to fine particles. The powder was further solubilize in hot water and then refluxed with 1 M NaOH for 6 hours at 50 °C. The solid remnants on the filter paper were weighed and discarded. The solvent was further used for corrosion inhibition experiments.

2.2. Materials

Aluminium 7075 alloy with density 2.83 g/cm^3 and composition (wt %): Si 0.41; Ti ≤ 0.20; Mn ≤ 0.30; Cu 1.38; Mg 2.62; Zn 5.89; Fe 0.50; and rest Al was utilized altogether for experimental and surface tests. Aluminium alloy samples with size of 30 mm × 3 mm × 3 mm were exposed to the aggressive solution in the electrochemical tests. The specimens were abraded according to ASTM A262, and cleaned following the ASTM G-1 standard. The test solution of 1 M NaOH was organized using research grade NaOH with distilled H_2O.

2.3. Electrochemical tests

Gamry workstation was connected to the three cell assembly with aluminium alloy (working electrode), platinum electrode (auxiliary electrode) and saturated calomel electrode (reference electrode) to carry out the electrochemical tests. All the obtained data was analyses through Echem analyst software

delivered by Gamry devices. EIS measurements were conducted under static conditions from 100 kHz to 0.01 Hz, with an amplitude of 10 mV. All potentials reported were measured in the range +250 mV – 250 mV versus reference electrode Polarization curves were carried out at a scan rate of 1.0 mVs^{-1}. The tests were conducted when the system showed a stable potential with and without inhibitor. The efficiency of inhibition is obtained using the equation below:

$$\eta\% = \frac{R_{ct(inh)} - R_{ct}}{R_{ct(inh)}} \times 100 \quad (8)$$

Where $R_{ct(inh)}$ and R_{ct} be the charge transfer resistance with and without inhibitor in 1M NaOH medium. The values of corrosion current density (I_{corr}) can be used to calculate the efficiency of inhibition (η %) through the equation below:

$$\eta\% = \frac{I_{corr} - I_{corr(i)}}{I_{corr}} \times 100 \quad (9)$$

Where I_{corr} and $I_{corr(i)}$ be the corrosion current density with and without inhibitor.

2.4. Surface Investigation

2.4.1. Scanning Electrochemical Microscopy (SECM)

A workstation of CHI900C was operated with a platinum tip probe, equipped with reference electrode, working electrode and counter electrode. SECM was conducted where the current flows through the platinum tip towards the metal surface acting as conducting or insulating [29]. All the corrosion reaction takes place in the electrochemical cell when the tip comes near to the metal surface with and without inhibitor.

2.4.2. Scanning Electron Microscopy (SEM) and Energy-dispersive X-ray spectroscopy (EDX)

The aluminium samples were submerged in 1M NaOH solution for 6 hours with and without DT inhibitor. The samples were further cleaned with standard solutions, dried and kept in desiccator to remove humidity. These samples were further exposed to the TESCAN VEGA II XMH instrument to conduct the SEM-EDX tests.

2.5. Quantum chemical investigations

Quantum simulations are done to support the experimental data with the theoretical parameters. Simulations were conducted using Gaussian 09 software and figures were obtained using Gauss view 5.0 software. Density function theory (DFT) method with B3LYP module was chosen for all atoms. Highest occupied molecular orbital (HOMO), Lowest unoccupied molecular orbital (LUMO), and dipole moment (μ) were investigated [30].

3. RESULTS AND DISCUSSION

3.1. Electrochemical tests

3.1.1. Electrochemical Impedance Spectroscopy

Electrochemical impedance spectroscopy tests were conducted to examine the surface changes, kinetics and corrosion process of the aluminium in alkaline medium. This technique is highly reliable to get the information about the corrosion reactions taking place at the electrodes with and without inhibitor [31-33]. Nyquist plots of aluminium alloy in 1 M NaOH medium at different concentrations of DT are shown in Fig. 2. The plots of aluminium in 1M NaOH shows two capacitive loops at higher and lower frequency along with an inductive loop at medium frequency corresponding to typical Randles elements.

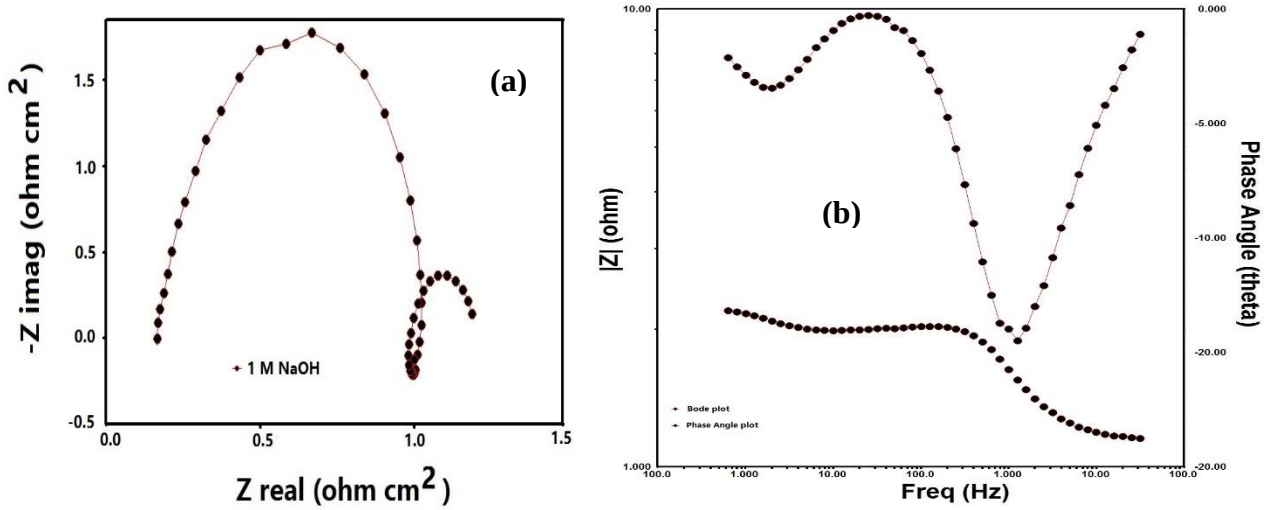

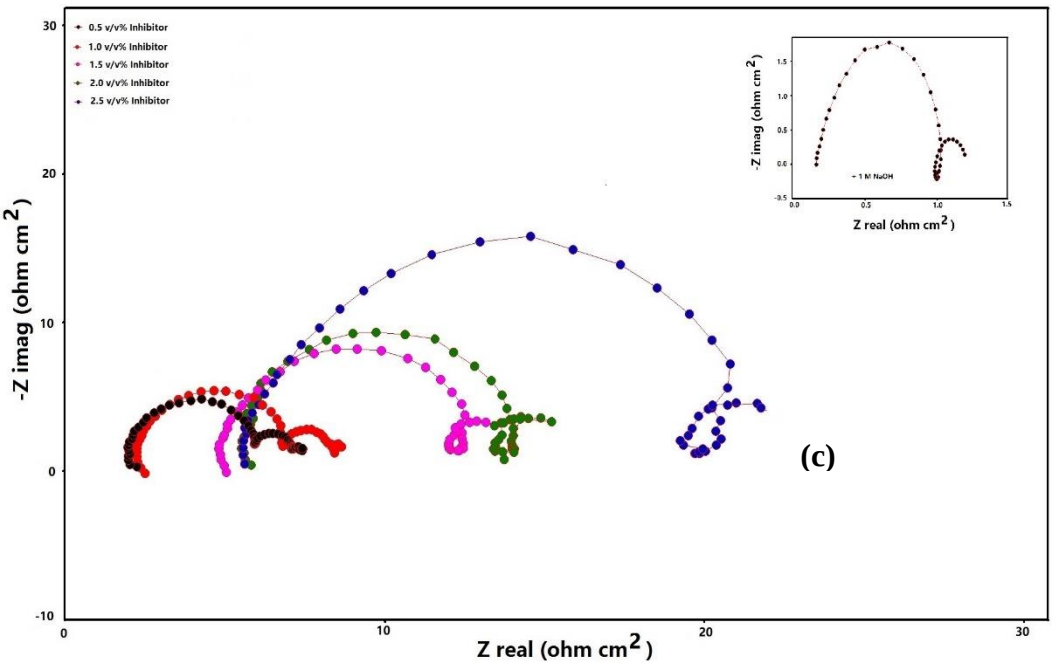

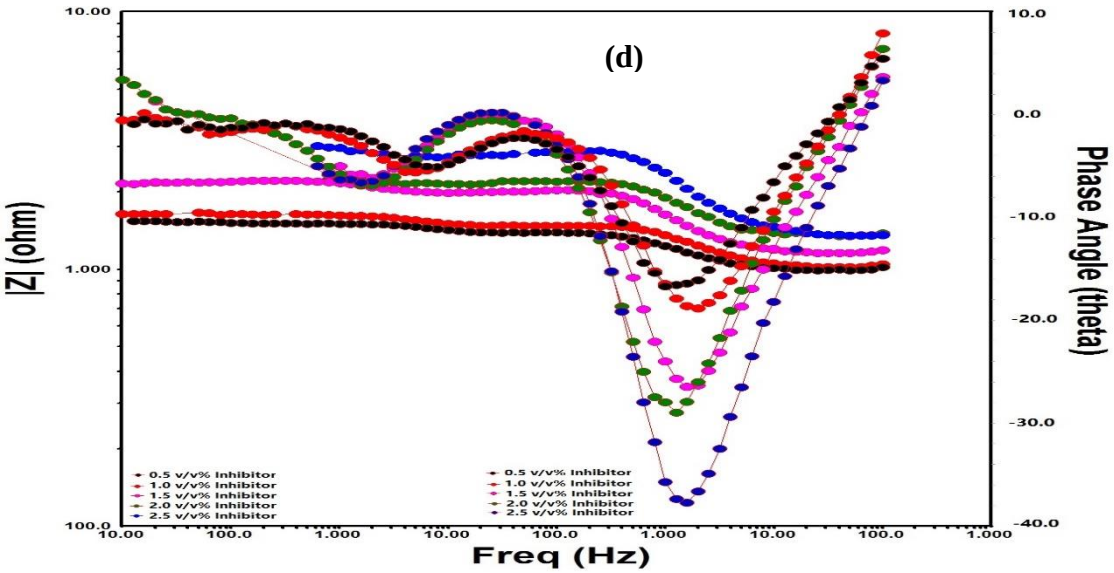

Figure 2. (a) Nyquist plot of 1M NaOH, (b) Bode-phase angle plot of 1M NaOH, (c) Nyquist plot of DT and (d) Bode-phase angle plot of DT inhibitor.

The impedance spectra (Fig. 2a) is characterized by a capacitive time constant at higher frequency (HF), second capacitive time constant at lower frequency (LF), separated by an inductive time constant at medium frequency (MF) values. The capacitive loop at HF is ascribed to the formation of protective (oxide) layer. According to Brett [34], the first capacitive time constant is associated with the reaction of aluminium oxidation at the metal/oxide/electrolyte interface. In this process, the formation of Al^{+} ions at the metal/ oxide interface and their migration through oxide layer to the oxide/solution interface occur due to high electric field strength, where they become oxidized to Al^{+3} . This is attributed to the fact that these processes determined by capacitive time constant could either be suggested by overlapping of time constants or by the assumption that one process dominates and, therefore, excludes the other processes [35]. The inductive loop at intermediate frequencies imputed to relaxation of the adsorbed intermediate species (OH^{-}) in the oxide layer, present on the metal surface. The presence of inductive loop is reported in literature. The second time constant of LF arises due to the adsorption and incorporation of hydroxide ions into the oxide film [36].

The prototype to fit the data consists of the solution resistance (R_s), the charge-transfer resistance (R_{ct1} and R_{ct2}), inductive components (R_L and L), and the constant phase angle component (CPE1 and CPE2) as represented in Fig. 3. CPE is further defined by two values, Q, n and are listed in Table 1.

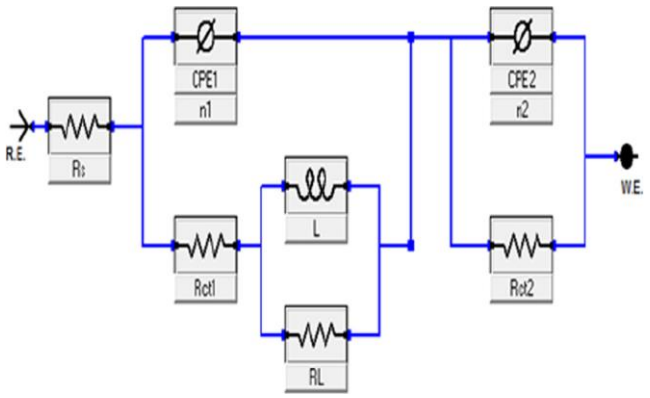

Figure 3. Corresponding model used to fit the data.

As illustrated in Table 1, the increase in the values of R_{ct} with rise in inhibitor concentration may be due to the presence of DT molecules on the metal surface. The inhibitor film covers the active centres, does not allows the corrosive solution to penetrate and thereby increases the resistance. Fig. 2 depicts bode and phase-angle plots of impedance. As is well established that the values of slope (*S*) and phase angle (α°) for perfect capacitor must be -1 and -90° respectively. In current study, the extreme slope value (-0.43), and highest phase angle (39°) is seen at 2.5% v/v concentration of DT inhibitor respectively. The approaching of *S* and α° values near the perfect capacitor discloses the adsorption of DT molecules above the aluminium alloy surface [37].

Table 1. Electrochemical impedance data for aluminium alloy in 1 M NaOH in the absence and presence of DT at 308 K.

Solution	R_s	$Q1$	n	R_{ct1}	L	R_L	$Q2$	R_{ct2}	C_{dl}	η
	Ω	($S\Omega^{-1}cm^{-2}$)	0.746	Ω cm^2	Hcm^2	Ω cm^2	($S\Omega^{-1}cm^{-2}$)	Ω cm^2	μF cm^{-2}	%
1M NaOH	0.8	470 X 10^{-6}	0.812	1.94	1.63	0.14	43 X 10^{-6}	0.6	477.5	--
DT 0.5%	1.5	188 X 10^{-6}	0.832	06.3	0.44	04.8	49 X 10^{-6}	0.7	112.6	69
DT 1.0%	1.4	167 X 10^{-6}	0.845	08.2	1.78	06.8	51 X 10^{-6}	0.3	98.5	76
DT 1.5%	1.4	149 X 10^{-6}	0.878	11.4	1.90	10.0	57 X 10^{-6}	0.7	77.5	83
DT 2.0%	1.5	135 X 10^{-6}	0.899	13.7	2.45	12.2	68 X 10^{-6}	0.4	71.3	86
DT 2.5%	1.4	84 X 10^{-6}	0.902	19.2	0.66	17.8	98 X 10^{-6}	0.8	57.5	90

As the charge transfer resistance values tend to increase with rise in DT concentration the values of double layer capacitance decreases. This phenomenon can be seen due to the development of film by the DT molecules on the aluminium surface. The R_{ct} values in absence of inhibitor are lower suggesting a lower resistance due to the penetration of aluminium surface by the alkaline solution. The greatest inhibition efficiency of 90% is been exhibited by DT inhibitor at 2.5% v/v concentration. Although, the efficiency did not changed much as the concentration was further increased to 3.0 and 3.5% v/v.

3.1.2. Potentiodynamic polarization tests

The corrosion potential (-E_{corr}), corrosion current density (I_{corr}), and anodic (β_a) and cathodic (β_c) slopes as attained by the potentiodynamic figures are presented in Table 2. The polarization plots for

aluminium alloy in 1M NaOH with and without DT are depicted in Fig. 4. As can be observed from Fig. 4 the cathodic curves are dominating due to the hydrogen evolution that is taking place. These dominating cathodic slopes are not surprising for aluminium and may take place due to the hydrogen evolution from the oxide or an oxide-inhibitor complex [38].

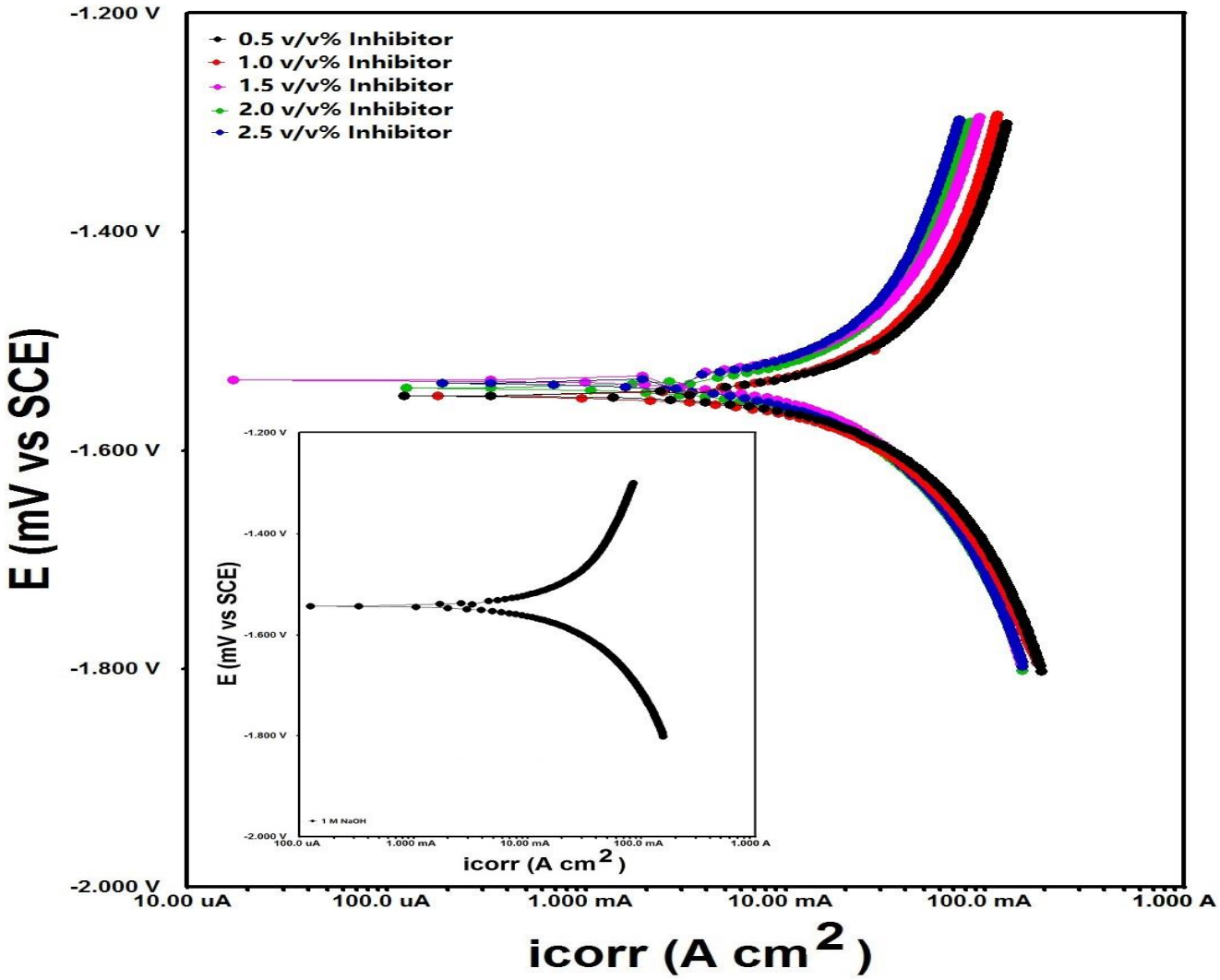

Figure 4. Potentiodynamic polarization plots for aluminium alloy in 1 M NaOH with and without DT inhibitor at 308 K.

This can draw an inference that the corrosion of aluminium in 1M NaOH medium is under cathodic control. The outcomes presented the decrease in I_{corr} for aluminium in 1M NaOH with DT inhibitor as compared to 1M NaOH solution without inhibitor. This could be due to the barrier of film formed by the DT molecules on the aluminium surface. The adsorption of DT molecules over aluminium reduces the rate of i_{corr} and increases η% as presented in Table 2.

Table 2. Potentiodynamic polarization parameters for aluminium metal in 1 M NaOH in the absence and presence of DT at 308 K.

Solution	$-E_{corr}$	i_{corr}	β_a	β_c	η
	mV/SCE	mA cm^{-2}	mV/dec	mV/dec	%
1M NaOH	1.845	106.7	511	1013	--
DT 0.5%	1.866	84.3	232	99	21
DT 1.0%	1.652	67.4	187	638	37
DT 1.5%	1.564	38.6	166	877	64
DT 2.0%	1.659	13.6	142	756	87
DT 2.5%	1.561	9.7	121	963	91

Al_2O_3 accompanying aluminium surface causes high passivity, but in alkaline aqueous medium it repassivate in presence of defects formed due to corrosion process. The corrosion can lead to the breakdown of the oxide layer from the aluminium surface in 1M NaOH medium [39]. So, the corrosion process was inhibited in presence of DT and maximum efficiency of 91% was observed at 2.5% v/v concentration.

3.2. Surface Investigation

3.2.1. SECM

The electrochemical information about the localized corrosion taking place at the metal surface can be determined using SECM. This technique has proved to be very useful in recent years due to its accuracy and very helpful in predicting corrosion mechanisms. One of the benefit of using SECM is that it can incorporate both insulating (coated / films) and conducting (non-coated) surfaces. This can help in comparison of both the surfaces in different mediums and can help to derive a suitable mechanism of action [40].

A probe approach curve is done before the start of each test to establish the same distance for each exposed samples. As the tip aligns the metal surface the changes in current of the system can be observed [41]. All the metal samples were submerged in the corrosive medium for 20 minutes before the start of tests.

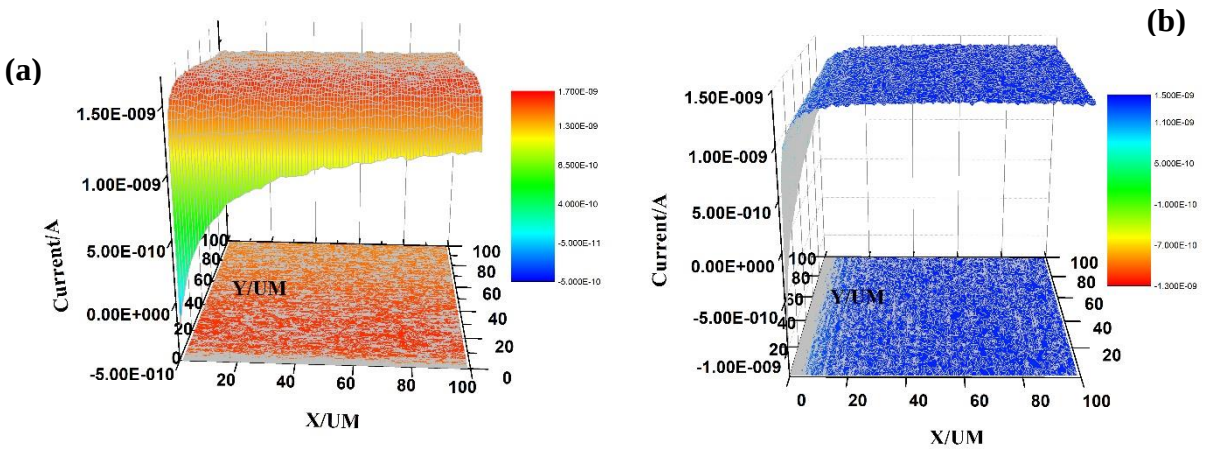

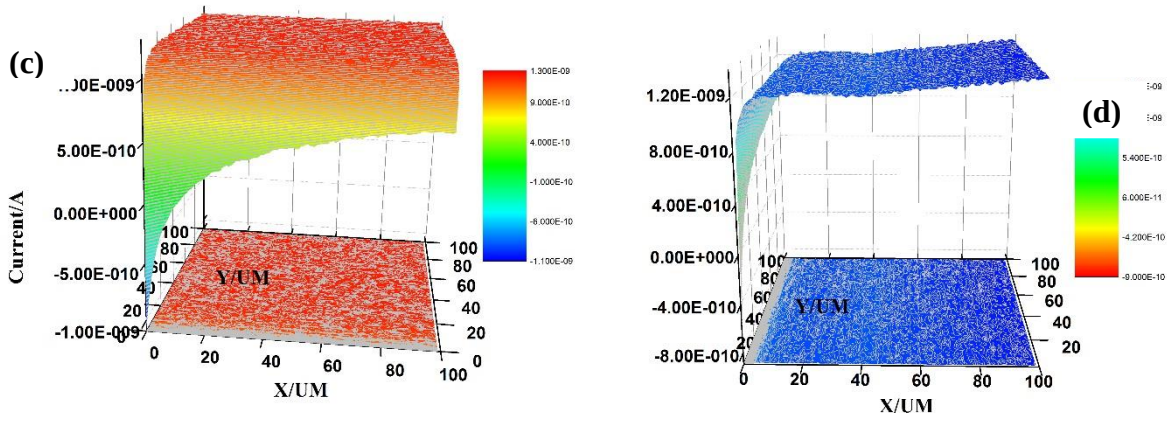

Figure 5. (a) 3D x-axis plot of AA in 1M NaOH, (b) 3D y-axis plot of AA in 1M NaOH, (c) 3D x-axis plot of AA in DT and (d) 3D y-axis plot of AA in DT inhibitor.

The 3D images of SECM test for aluminium in 1M NaOH with and without DT is shown in Fig. 5. As the probe tip comes near the aluminium surface without inhibitor, rise in current is perceived due to the conducting behavior of aluminium. Here, as the tip is in straight contact with the metal surface, the conducting activity is observed vindicated by the increase in current on both x and y axis as shown in Fig. 5a, 5b. On the other hand, when the probe comes near the metal surface with DT inhibitor the current is reduced as the metal begins to act as insulating surface. This is due to the existence of DT inhibitor film on the aluminium surface in 1 M NaOH medium that forms a protective layer and inhibits the corrosive solution on both x and y axis as displayed in Fig. 5c, 5d. After the comparison of currents across x axis and y axis for samples with DT inhibitor and samples without DT inhibitor, the effective corrosion inhibition of DT molecules for aluminium in NaOH medium can be confirmed.

3.2.2. SEM-EDX

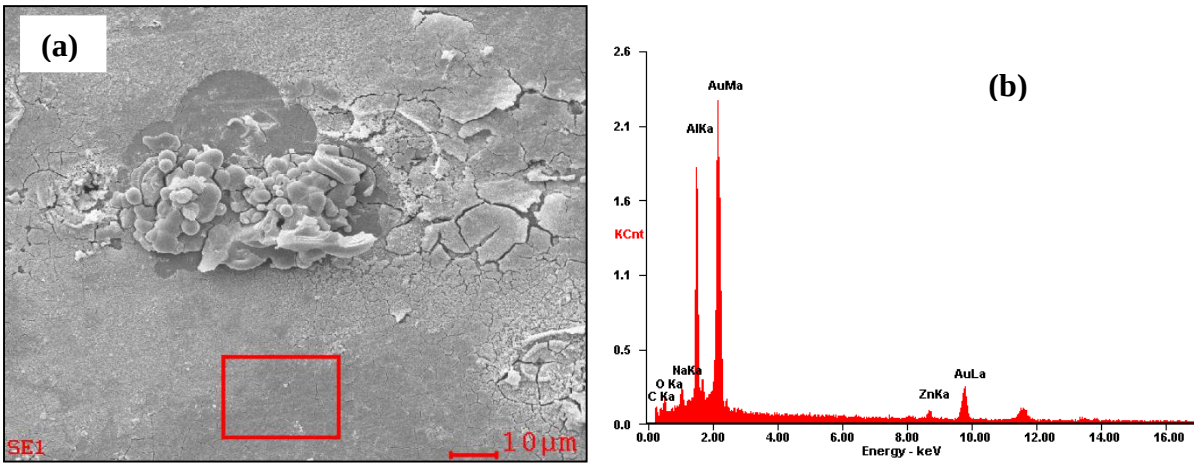

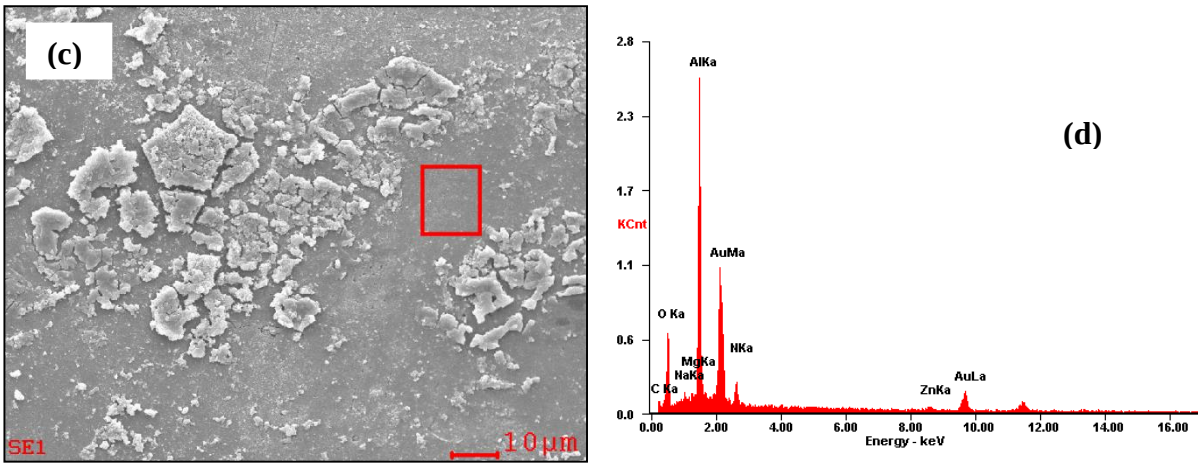

Figure 6. (a) SEM image of aluminium alloy in 1M NaOH, (b) EDX spectra of Aluminium alloy in 1M NaOH, (c) SEM image of aluminium alloy in 1M NaOH with 2.5% DT (d) EDX spectra of Aluminium alloy in 1M NaOH with 2.5% DT inhibitor.

The aluminium samples were immersed in NaOH solution with and without DT for 6 hours, dried and exposed to the instrument for tests. Fig. 6a-d shows the images of aluminium surface to confirm the positive inhibition of DT inhibitor in NaOH solution.

Fig. 6a depicts a corroded and ruptured surface with cracks. The upper layer of the aluminium metal can be seen to be deteriorated due to corrosion in NaOH solution. The EDX spectra shows the peaks of element present on the surface (Fig. 6b). Though, with DT inhibitor (Fig. 6c), the corrosion of Al alloy is diminished remarkably. The oxide deposits can be seen on the surface but overall surface is smooth as compared to blank. The EDX spectra also shows extra elements present over the surface due to the presence of inhibitor film (Fig. 6d). Consequently, the inhibitor adsorbed on the surface of aluminium alloy exhibits smooth texture and prevents the surface from corrosion.

3.2.3. Quantum Chemical Investigations

The simulations were run to find the optimized geometry for the inhibitor. After the optimized geometry was obtained further studies were performed to get the detailed information about the molecular orbitals. The obtained computational structures are displayed in Fig. 7. Fig. 7a shows the optimized geometry, Fig.7b shows the electronic charge distribution, Fig. 7c show the highest occupied molecular orbital (HOMO), and Fig. 7d shows the lowest unoccupied molecular orbital (LUMO) structures. Likewise, the obtained parameters including E_{HOMO}, E_{LUMO}, ΔE ($_{LUMO-HOMO}$), dipole moments (μ) are enumerated in Table 3. HOMO and LUMO represents the active sites through which the nucleophilic and electrophilic substitution reactions takes place. In other words, these sites provide the information about the electron donor and electron acceptor atoms in the inhibitor molecule.

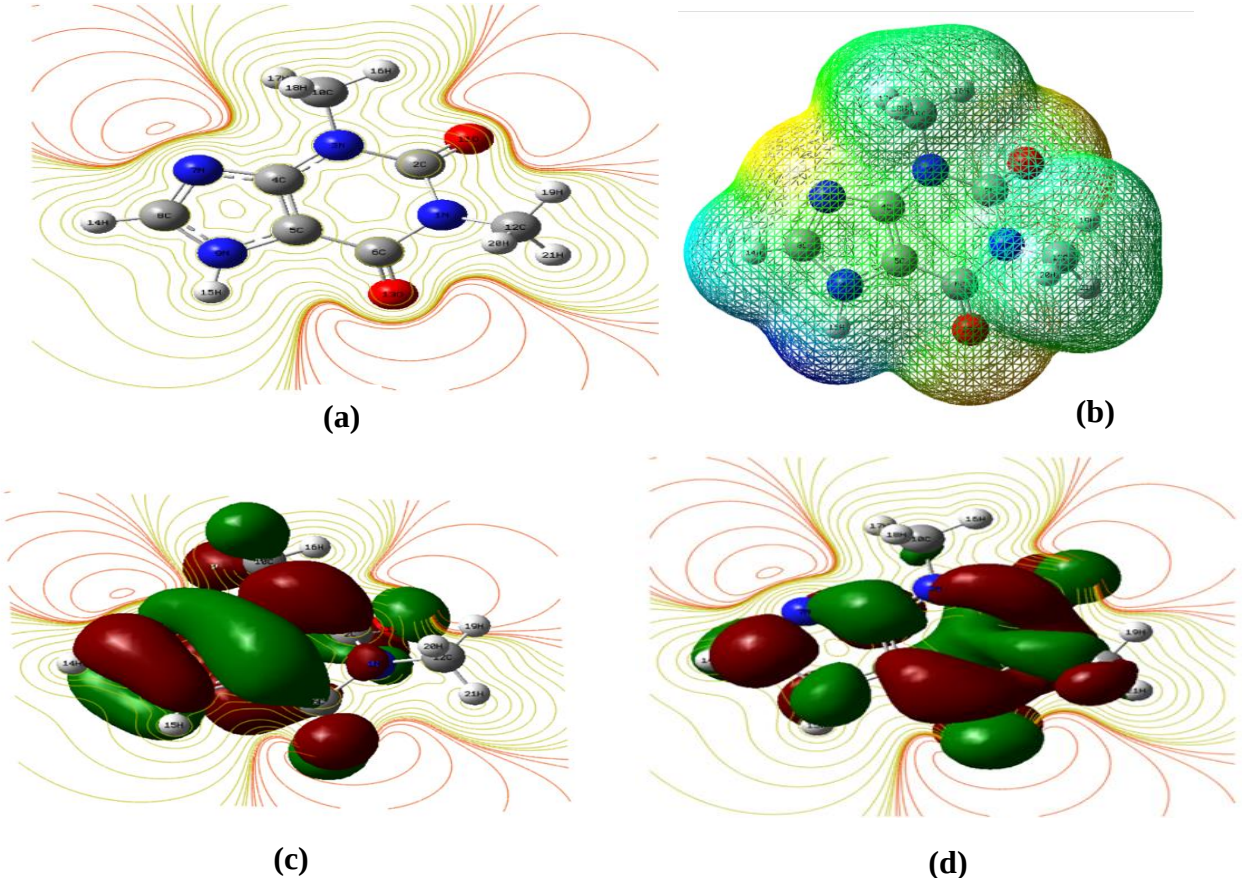

Figure 7. (a) Optimized molecular structure (b) total charge density (c) HOMO and (d) LUMO molecular orbital density distribution of DT.

Table 3. Computational parameters of DT Inhibitor using Gaussian 09 software.

Quantum Parameters	DT Inhibitor
HOMO (eV)	-5.656
LUMO (eV)	-1.077
ΔE (eV)	4.579
Dipole Moment (μ)	3.6437

The computational studies indicate towards the HOMO values that shows the electron donating tendency to the molecules ready to accept with vacant and low energy orbital. Meanwhile, the LUMO values indicate the inclination to accept electrons being the lower unoccupied orbitals [42]. The reactivity of the DT molecules towards the aluminium surface is represented by the energy gap ΔE that serves to be an important parameter. The computational calculations also confirm the relocation of electrons from the DT molecules to the aluminium surface leading to the bond formation that inhibits corrosion [43-45].

4. CONCLUSIONS

- DT can be used as potential inhibitor for corrosion of aluminium alloy 1 M NaOH solution.
- The impedance studies revealed that the charge transfer resistance rises in presence of DT and double layer capacitance values decreases.
- Polarization studies pointed that the cathodic shifts are dominating.
- SEM-EDX showed the smooth texture of the aluminium alloy in presence of DT.
- Computational studies well supported the experimental findings.

ACKNOWLEDGEMENTS
The authors are grateful to the funds by Ministry of Science and Technology of China Petrochemical Group project-P18022-1, Sichuan 1000 Talent Fund, and Youth Scientific and Innovation Research Team for Advanced Surface Functional Materials, Southwest Petroleum University, number 2018CXTD06.

References

1. Junlei Wang, Fuping Xiong, Hongwei Liu, Tiansui Zhang, Yanyan Li, Chenjing Li, Wu Xia, Haitao Wang, Hongfang Liu, *Bioelectrochem*. 129 (2019) 10.
2. Ambrish Singh, Yuanhua Lin, Wanying Liu, Shijie Yu, Jie Pan, Chengqiang Ren, Deng Kuanhai, *J. Ind. Eng. Chem*. 20 (2014) 4276.
3. Amjad Saleh El-Amoush, *J. Alloys Compd.* 443 (2007) 171.
4. M. Navaser, M. Atapour, *J. Mater. Sci Tech*. 33 (2017) 155.
5. Vaibhav Pandey, J. K. Singh, K. Chattopadhyay, N. C. Santhi Srinivas, Vakil Singh, *J. Alloys Compd.* 723 (2017) 826.
6. Rasiha Nefise Mutlu, Sevgi Ateş, Birgül Yazıcı, *Int. J. Hyd. Ener*. 42 (2017) 23315.
7. A.C. Umamaheshwer Rao, V. Vasu, M. Govindaraju, K.V. Saisrinadh, *T. Nonferr. Metal. Soc*. 26 (2016) 1447.
8. B. Davó A.Conde J.de Damborenea, *Corros. Sci*. 48 (2006) 4113.
9. M. Rashvand avei, M. Jafarian, H. Moghanni Bavil Olyaei, F. Gobal, S. M. Hosseini M. G. Mahjani, *Mater. Chem. Phys*. 143 (2013) 133.
10. Urša Tiringer, Janez Kovač, Ingrid Milošev, *Corros. Sci*. 119 (2017) 46.
11. Li Jin-feng, Peng Zhuo-wei, Li Chao-xing, Jia Zhi-qiang, Chen Wen-jing, Zheng Zi-qiao, *T. Nonferr. Metal. Soc*. 18 (2008) 755.
12. Klodian Xhanari, Matjaz Finsgar, *Arab. J. Chem*. (2016) http://dx.doi.org/10.1016/j.arabjc.2016.08.009.
13. S. M. Moon, S. I. Pyun, *Electrochim. Acta* 44 (1999) 2445.
14. I.B. Obot, N.O. Obi-Egbedi, S.A. Umoren, *Corros. Sci*. 51 (2009) 1868.
15. Gokhan Gece, *Corros. Sci*. 53 (2011) 3873.
16. Ileana Rotaru, Simona Varvara, Luiza Gaina, Liana Maria Muresan, *Appl. Surf. Sci*. 321 (2014) 188.
17. M. Abdallah, E.A.M. Gad, M. Sobhi, Jabir H. Al-Fahemi, M.M. Alfakeer, *Egypt. J. Petrol*. 28 (2019) 173.
18. Mahmoud N. El-Haddad, A.S. Fouda, A.F. Hassan, *Chem. Data. Collec*. 22 (2019) 100251.
19. Priyanka Singh, D.S. Chauhan, S.S. Chauhan, G. Singh, *J. Mol. Liq*. 286 (2019) 110903.
20. M. Abdallah, I. Zaafarany, J.H. Al-Fahemi, Y. Abdallah, A.S. Fouda, *Int. J. Electrochem Sci*. 7 (2012) 6622.

21. Ahmed Abdel Nazeer, H.M. El-Abbasy, A.S. Fouda, *Res. Chem. Intermed*. 39 (2013) 921.
22. K.N. Mohan, S.S. Shiva Kumar, A.M. Badie, *J. Korean Chem. Soc*. 55 (2011) 364.
23. N. Vaszilcsin, V. Ordodi, A. Borz, *Int. J. Pharm*. 431 (2012) 241.
24. R. Solmaz , G. Kardas , B. Yazici , M. Erbil , *Prot. Met*. 43 (2007) 476.
25. A. Samide, B. Tutunaru, C. Negrila, *Biochem. Eng*. 25 (2011) 299.
26. I. Ahamad, M. Quraishi, *Corros. Sci*. 52 (2010) 651.
27. D.Q. Zhanga, Q.R. Cai, X.M. He, L.X. Gao, G.S. Kim, *Mater. Chem. Phys*. 114 (2009) 612.
28. X. Xu, A. Singh, Z. Sun, K.R. Ansari, Y. Lin, *R. Soc. Open Sci*. 4 (2017) 170933.
29. A. Singh, Y. Lin, M. A. Quraishi, O. L. Olasunkanmi, O. E. Fayemi, Y. Sasikumar, B. Ramaganthan, I. Bahadur, I. B. Obot, A. S. Adekunle, M. M. Kabanda, E. E. Ebenso, *Molecules*, (2015) 2015122.
30. 30. Gaussian, M.J. Frisch, G.W. Trucks, H.B. Schlegel, G.E. Scuseria, M.A. Robb, J.R. Cheeseman, Jr. J.A. Montgomery, T. Vreven, K.N. Kudin, J.C. Burant, J.M. Millam, S.S. Iyengar, J. Tomasi, V. Barone, B. Mennucci, M. Cossi, G. Scalmani, N. Rega, G.A. Petersson, H. Nakatsuji, M. Hada, M. Ehara, K. Toyota, R. Fukuda, J. Hasegawa, M. Ishida, T. Nakajima, Y. Honda, O. Kitao, H. Nakai, M. Klene, X. Li, J.E. Knox, H.P. Hratchian, J.B. Cross, V. Bakken, C. Adamo, J. Jaramillo, R. Gomperts, R.E. Stratman, O. Yazyev, A.J. Austin, R. Cammi, C. Pomelli, J.W. Ochterski, P.Y. Ayala, K. Morokuma, G.A. Voth, P. Salvador, J.J. Dannenberg, V.G. Zakrzewski, S. Dapprich, A.D. Daniels, M.C. Strain, O. Farkas, D.K. Malick, A.D. Rabuck, K. Raghavachari, J.B. Foresman, J.V. Ortiz,Q. Cui, A.G. Baboul, S. Clifford, J. Cioslowski, B.B. Stefanov, G. Liu, Liashenko, A .P. Piskorz, I.Komaromi, R.L. Martin, D.J. Fox, T. Keith, M.A. Al-Laham, C.Y. Peng, A. Nanayakkara, M. Challacombe, P.M.W. Gill, B. Johnson, W. Chen, M.W. Wong, C. Gonzalez, J.A. Pople, Gaussian, Inc., Wallingford CT, (2018).
31. A. Singh, I. Ahamad, M. A. Quraishi, *Arab. J. Chem*. 9 (2016) S1584.
32. Ambrish Singh, K. R. Ansari, M. A. Quraishi, Hassane Lgaz and Yuanhua Lin, *J. Alloys Comp*. 762 (2018) 347.
33. A. Singh, Y. Lin, W. Liu, D. Kuanhai, J. Pan, B. Huang,C. Ren, D. Zeng, *J. Tai. Inst. Chem. E*. 45 (2014) 1918.
34. C.M.A. Brett, *Portug. Electrochim. Acta.* 7 (1989) 123.
35. K.F. Khaled, *Corros. Sci*. 52 (2010) 2905.
36. J.B. Bessone, D.R. Salinas, C.E. Mayer, E. Ebert, W.J. Lorenz, *Electrochim. Acta*. 37 (1992) 2283.
37. M.A. Quraishi, A. Singh, V.K. Singh, D.K. Yadav, A.K. Singh, *Mater. Chem. Phys*. 122 (2010) 114.
38. A. Singh, I. Ahamad, V.K. Singh, M.A. Quraishi, *J. Sol. State Electrochem*. 15 (2011) 1087.
39. Ambrish Singh, K.R. Ansari, Jiyaul Haque, Parul Dohare, Hassane Lgaz, Rachid Salghi, M.A. Quraishi, *J. Taiwan Inst. Chem. E*. 82 (2018) 233.
40. Ambrish Singh, Y. Lin, I. B. Obot, E. E. Ebenso, K. R. Ansari, M. A. Quraishi, *Appl. Surf. Sci*. 356 (2015) 341.
41. A. Singh, Y. Lin, E. E. Ebenso, W. Liu, B. Huang, *Int. J. Electrochem. Sci*. 9 (2014) 5993.
42. A. Singh, E. E. Ebenso, M. A. Quraishi, Y. Lin, *Int. J. Electrochem. Sci*. 9 (2014) 7495.
43. A. Singh, K.R. Ansari, A. Kumar, W. Liu, C. Songsong, Y. Lin, *J. Alloys Comp*. 712 (2017) 121.
44. A. Singh, Y. Lin, E. E. Ebenso, W. Liu, J. Pan, B. Huang, *J. Ind. Eng. Chem*. 24 (2015) 219.
45. A. Singh, Yuanhua Lin, K. R. Ansari, M. A. Quraishi, E. E. Ebenso, Songsong Chen, W. Liu, *Appl. Surf. Sci*. 359 (2015) 331.

© 2020 The Authors. Published by ESG (www.electrochemsci.org). This article is an open access article distributed under the terms and conditions of the Creative Commons Attribution license (http://creativecommons.org/licenses/by/4.0/).